crystals

MDPI

Article

Two Organic Cation Salts Containing Tetra(isothiocyanate)cobaltate(II): Synthesis, Crystal Structures, Spectroscopic, Optical and Magnetic Properties

Zheng Zhang [1], Junwei Xu [2], Sisi Yan [2], Yangli Chen [2], Yan Wang [1], Zhuo Chen [1,*] and Chunlin Ni [2,*]

[1] Department of Materials Science and Engineering, School of Aeronautics and Astronautics, Central South University, Changsha 410012, China; zzhengchem@163.com (Z.Z.); wangyan@csu.edu.cn (Y.W.)

[2] College of Materials and Energy, Institute of Biomaterial, South China Agricultural University, Guangzhou 510642, China; W916173004@sina.com (J.X.); Lines_end@126.com (S.Y.); yanglichen2016@126.com (Y.C.)

* Correspondence: cz2009@csu.edu.cn (Z.C.); niclchem@scau.edu.cn (C.N.); Tel.: +86-731-8887-7495 (Z.C.); +86-20-38295132 (C.N.); Fax: +86-731-8883-0945 (Z.C.); +86-20-85285026 (C.N.)

Academic Editor: Sławomir J. Grabowski
Received: 13 January 2017; Accepted: 17 March 2017; Published: 22 March 2017

Abstract: Single crystals of two hybrid organic-inorganic molecular solids, benzyl pyridinium tetra(isothiocyanate)cobalt ($[BzPy]_2[Co(NCS)_4]$) (**1**) and benzyl quinolinium tetra(isothiocyanate)cobalt ($[BzQl]_2[Co(NCS)_4]$) (**2**), were grown using a slow evaporation growth technique at room temperature and their IR, UV-Vis, X-ray crystal structures, luminescence, and magnetism were reported. The crystal structural analysis revealed that two molecular solids crystallize in the monoclinic space group $P2_1/c$ of **1** and $P2_1/n$ of **2**. The cations form a dimer through weak C–H···π/π···π interactions in **1** and **2**, and the adjacent cation (containing N(6) atom) in **2** forms a columnar structure through π···π weak interactions between the quinoline and benzene rings, while the anions in **1** form a layer structure via short S···Co interactions. The anions (A) and cations (C) are arranged alternatively into a column in the sequence of ···A–CC–A–CC–A··· for **1**, while the two anions and cationic dimer in **2** form an alliance by the C–H···π, C–H···S and C–H···N hydrogen bonds. A weak S···π interaction was found in **1** and **2**. The two molecular solids show a broad fluorescence emission around 400 nm in the solid state at room temperature, and weak antiferromagnetic coupling behavior when the temperature is lowered.

Keywords: tetra(isothiocyanate)cobalt(II) anion; spectra; crystal structure; fluorescence; magnetic properties

1. Introduction

During the last two decades, hybrid organic-inorganic molecular materials based on organic cations and inorganic complex anions have played a major role in the development of advanced functional materials. They have attracted the interest of scientists due to their special structural features and physical properties, which include novel catalytic, non-linear optical, conductive, fluorescent and magnetic properties [1–7]. Among these compounds, the transition metal complexes anion (based on the thiocyanate or isothiocyanate ligand) attracts much interest as these ions may coordinate either through the N or S atom as a monodentate ligand, or though N and S atoms as a bridging ligand, forming some complexes with one-, two- or three-dimensional networks [4,8–10]. In particular,

the inherent coordination angle of the isothiocyanate species leads to a wide range of various molecular solids containing $[M(NCS)_4]^{2-}$ (M = Mn^{2+}, Co^{2+}, Zn^{2+}), which may exhibit interesting magnetic behaviors, electronic, and optical properties [11–15]. The selection of the counter organic cation is of key importance as it controls the stacking of the whole molecule, and the non-covalent interactions (such as weak $p\cdots\pi/\pi\cdots\pi$ stacking interactions and hydrogen bonds) also play an important role in the arrangement of the structural units of molecular solids [16–18]. Our previously published studies have been devoted to the syntheses, X-ray single crystal structures, spectroscopic studies, magnetic or fluorescent properties of hybrid materials based on the tetra(isothiocyanate)cobalt/zinc anion and substituted benzyl triphenylphosphonium cations. The examples of $[4RBzTPP]_2[Co(NCS)_4]$ (R = H, F, Br, NO_2) [19,20], $[3BrBzTPP]_2[Co(NCS)_4]$ (R = Br, CN) [21], $[2ClBzTPP]_2[Co(NCS)_4]$ and $[4ClBzTPP]_2[Co(NCS)_4]$ [22] and $[4RBzTPP]_2[Zn(NCS)_4]$ (R = H, NO_2) [23] illustrate the importance of the size of the counterion. In our recent report on $[4NO_2BzPy]_2[Co(NCS)_4]$ [24], the $[Co(NCS)_4]^{2-}$ anions formed an unusual layer structure through S···N and S···Co interactions, and the $[4NO_2BzPy]^+$ cations were stacked into a 1D column by the weak $p\cdots\pi$ interactions. These observations have sparked our continuing research interest, and therefore, in this work, we introduced benzyl pyridinium ($[BzPy]^+$) and benzyl quinolinium ($[BzQl]^+$) into the system containing $[Co(NCS)_4]^{2-}$ anions and obtained two new hybrid materials, $[BzPy]_2[Co(NCS)_4]$ **1** and $[BzQl]_2[Co(NCS)_4]$ **2**, whose crystal structures, spectroscopic, optical and magnetic properties have been investigated. It is of much interest that two solids exhibit dual functionalities such as antiferromagnetic behavior and luminescent activity.

2. Results and Discussion

2.1. Single Crystal XRD and Powder XRD

The structural analysis of **1** and **2** were carried out on grown crystals using a Bruker SMART APEX (Göttingen, Germany) X-ray diffractometer at 291 K. $[BzPy]_2[Co(NCS)_4]$ (**1**) crystallizes in monoclinic system with $P2_1/c$ space group, whose asymmetric cell unit consisted of one $[Co(NCS)_4]^{2-}$ anion and two $[BzPy]^+$ cations (Figure 1a). The $[Co(NCS)_4]^{2-}$ anion exhibits a distorted tetrahedral coordination geometry with an average Co-N bond distance of 1.952(3) Å and an average N–Co–N bond angle of 107.20(12)°. Some important bond lengths and bond angles are listed in Table 1, and these values agree with reported molecular solids comprised of $[Co(NCS)_4]^{2-}$ anions [18,24]. Two $[BzPy]^+$ cations adopt a formation in which one pyridine ring and one phenyl ring are twisted with respect to a C–C–N reference plane. In the $[BzPy]^+$ cation moiety containing the N(5) atom, the dihedral angles subtended by the phenyl ring and pyridine ring make with the reference plane (defined by C(10)−C(11)−N(5)) are 31.4(2)° (θ_1) and 68.5°(2) (θ_2), respectively, while the phenyl and pyridine rings make a dihedral angle of 83.3(2)° (θ_3). For the $[BzPy]^+$ cation moiety containing the N(6) atom, the θ_1, θ_2 and θ_3 are 52.7(2)°, 66.9(2)° and 84.2(2)°, respectively.

As seen in Figure 1b, the $[Co(NCS)_4]^{2-}$ anions formed a layer structure through S···Co short interactions (the S(4)···Co(1A) and S(3B)···Co(1) distances of 4.205(2) and 4.032(2) Å) along the *ac*-direction [25,26]. The nearest Co···Co distance was 8.749 Å. It was found that the neighboring cations containing the N(5) atom formed a dimer through C−H···π weak interactions (Figure 2a), and the H(16) to the centroid of the C(5)–C(10) ring distance (d1) was 2.923(2) Å. As seen in Figure 2b, π···π interactions were present between the phenyl (molecule with N6) and the pyridyl (molecule with N5) rings in the crystals, with a distance 3.550(2) Å. Figure 2c shows the $[Co(NCS)_4]^{2-}$ anions with the cationic dimers (containing a N(5) atom, denoted as C_1C_1) in alternate stacks forming an alternating columnar structure in a $\cdots A–C_1C_1–A–C_1C_1\cdots$ sequence through C(7)–H(7)···N(4) (d2 = 2.810(2) Å) and C(11)–H(11A)···N(2) (d3 = 2.953(2) Å) hydrogen bonds. Amid the anions and cations (C_2) containing the N(6) atom (Figure 2d), there existed a S···π interaction(d4) (S(1) to the centroid of the C(17B)–C(22B) ring distance of 3.714(2) Å) and C(20)–H(20)···N(4) hydrogen bond (Table 2). The regular stacks between anions and cations resulted in the formation of the 3D network of **1** (Figure S1).

Table 1. Selected bond lengths and bond angles for **1** and **2**.

Compound	1	2
Bond length (Å)		
Co(1)–N(1)	1.937(3)	1.958(3)
Co(1)–N(2)	1.945(3)	1.941(4)
Co(1)–N(3)	1.968(3)	1.966(3)
Co(1)–N(4)	1.957(3)	1.987(4)
N(1)–C(1)	1.138(5)	1.141(5)
N(2)–C(2)	1.146(5)	1.144(5)
N(3)–C(3)	1.162(4)	1.111(5)
N(4)–C(4)	1.159(5)	1.137(5)
S(1)–C(1)	1.609(4)	1.610(3)
S(2)–C(2)	1.611(4)	1.614(4)
S(3)–C(3)	1.599(4)	1.628(4)
S(4)–C(4)	1.610(4)	1.620(4)
Bond angles (°)		
N(1)–Co(1)–N(2)	115.60(12)	109.48(14)
N(1)–Co(1)–N(3)	106.98(12)	110.66(15)
N(1)–Co(1)–N(4)	110.11(12)	105.50(15)
N(2)–Co(1)–N(3)	110.20(12)	109.80(14)
N(2)–Co(1)–N(4)	105.08(12)	117.37(16)
N(3)–Co(1)–N(4)	108.75(12)	103.81(14)
Co(1)–N(1)–C(1)	173.2(3)	177.0(3)
Co(1)–N(2)–C(2)	171.5(3)	172.6(4)
Co(1)–N(3)–C(3)	172.2(3)	168.8(3)
Co(1)–N(4)–C(4)	173.2(3)	161.0(3)
N(5)–C(11)–C(10)	112.4(3)	114.6(3)

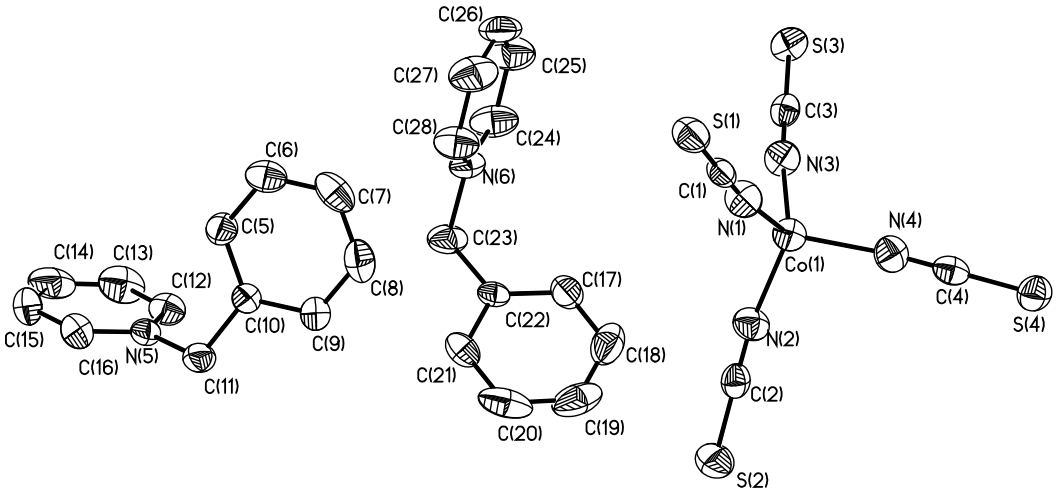

(**a**)

Figure 1. *Cont.*

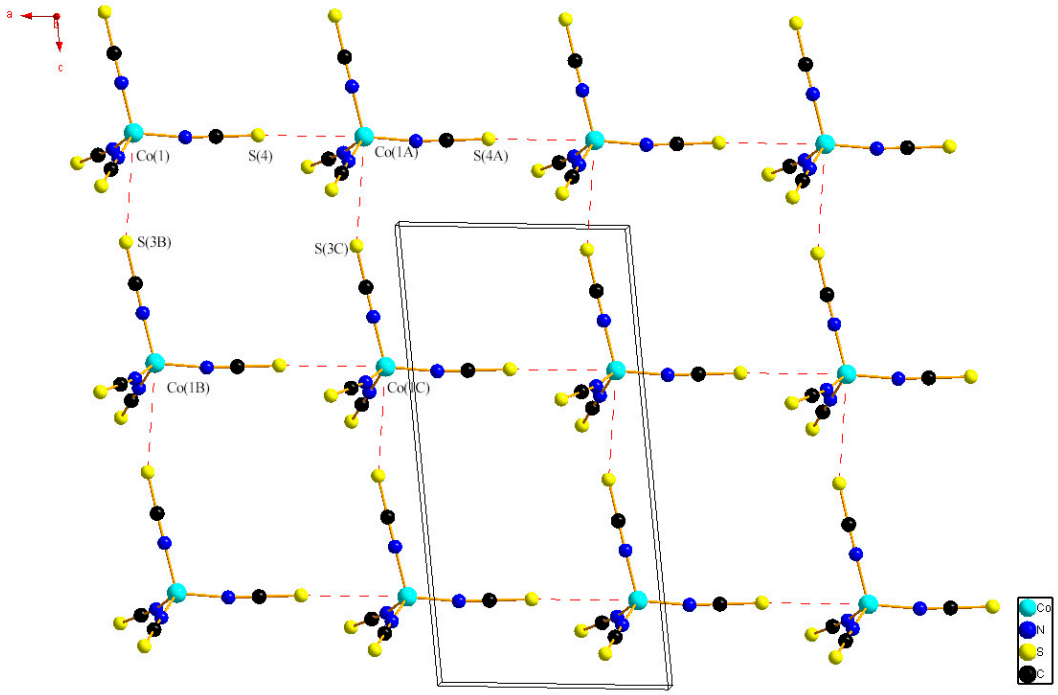

(**b**)

Figure 1. (**a**) Oak Ridge Thermal Ellipsoid Plot (ORTEP) plot (30% probability ellipsoids) showing the molecule structure of **1**. (**b**) The 2D layered structure of $[Co(NCS)_4]^{2-}$ through S···Co interaction between anions for **1**.

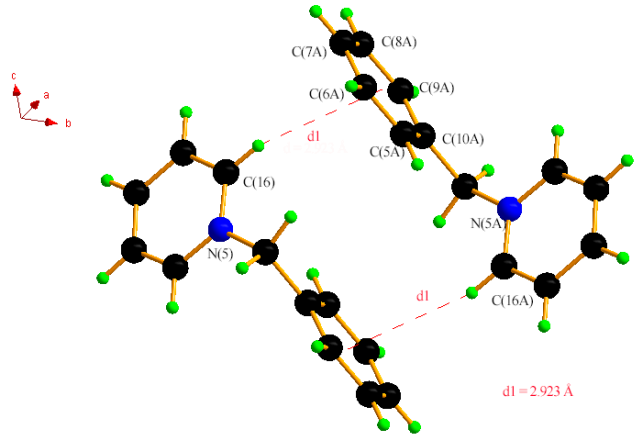

(**a**)

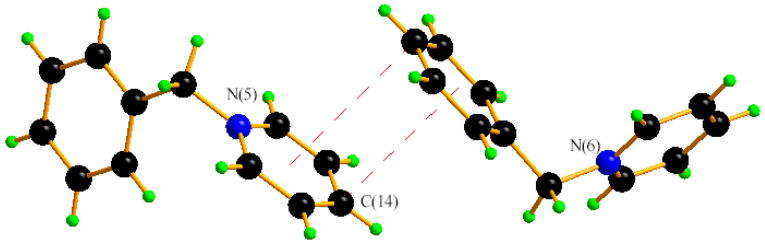

(**b**)

Figure 2. *Cont.*

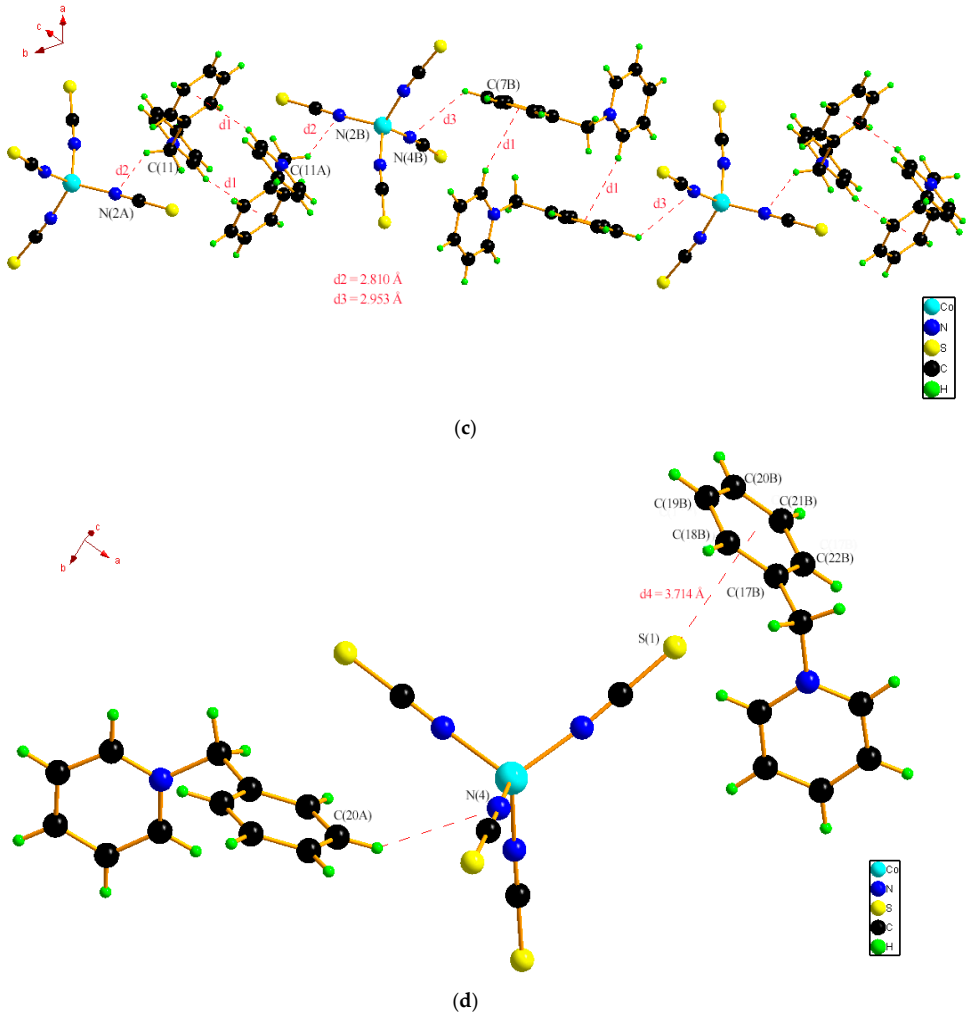

Figure 2. (**a**) A dimer formed through C–H···π interactions between the cations (C_1) of **1**. (**b**) The π···π interactions between the cations (C_1 and C_2) of **1**. (**c**) The 1D chain in ···A–C_1C_1–A–C_1C_1···sequence through C–H···N hydrogen bonds between the anions and cations (C_1) of **1**. (**d**) The S···π and C–H···N interactions between the anions and cations (C_2) of **1**.

Table 2. The parameters (Å, °) of hydrogen bonds in **1** and **2**.

D—H···A	*d* (D—H)	*d* (H···A)	*d* (D···A)	<(DHA)
Compound **1**				
C(7)–H(7)···N(4)#1	0.970	2.953	3.568(4)	124.0
C(20)–H(20)···N(4)#2	0.930	2.871	3.668(3)	144.0
Compound **2**				
C(9)–H(9)···N(5)	0.930	2.588	2.920(5)	101.0
C(11)–H(11B)···S(3)#3	0.970	2.753	3.700(4)	166.0
C(13)–H(13)···N(2)#4	0.930	2.926	3.648(4)	130.0
C(14)–H(14)···N(3)#4	0.930	2.995	3.660(4)	136.0

Symmetry transformations used to generate equivalent atoms: #1 = $-x + 1, -y + 1, -z + 1$; #2 = $x - 1, -y + 1/2, z - 1/2$; #3 = $x, y - 1, z$; #4 = $-x, -y + 1, -z$.

Every unit cell of **2** contains one $[Co(NCS)_4]^{2-}$ anion and two $[BzQl]^+$ cations. In the $[Co(NCS)_4]^{2-}$ anion, the average distance of Co–N bonds was 1.963(3), and the average N–Co–N bit angle was 108.86(15)°. These values are slightly bigger than those in **1**. The dihedral angles θ_1, θ_2, and θ_3 of the $[BzQl]^+$ cation are 166.7(1)°, 82.7(1)°, 85.3(1)° for the cations containing the N(5) atom, and 132.2(1)°,

78.9(1)°, 78.2(1)° for the cations containing the N(6) atom. These values are obviously different from those in **1**. In the $[Co(NCS)_4]^{2-}$ anions of **2**, the nearest Co···Co distance was 8.503(2) Å. The $[BzQl]^+$ cations show an orderly stacking structure, for example, the cations containing the N(5) atom (C_1) formed a dimer (Figure 3a) through π···π weak interactions between the quinoline rings in which the centroid of two quinoline rings distance was 3.787(2) Å (d1); while the cations containing the N(6) atom (C_2) formed a chain (Figure 3b) through π···π weak interactions between the quinoline and benzene rings with a distance of 3.518(2) Å (d2). These ordered arrangements between the cations in **2** may be attributed to the bigger delocalized π conjugated system of the quinoline ring which can easily form π···π weak interactions when the pyridine ring of **1** changed to the quinoline ring of **2** in the cation. An interesting structure was found where a cationic dimer was surrounded by two $[Co(NCS)_4]^{2-}$ anions, and formed an alliance via the C–H···N and C–H···S hydrogen bond (Figure 4a and Table 2). In addition, the S···π interactions [21], (the S(1) to centroid of C(5)–C(10) ring distance of 3.708(2) Å (d3)) and C(33)–H(33)···S(1) hydrogen bonds with a C(33)℘?℘S(1) distance of 3.701(2) Å were found between the anions and the cations (Figure 4b). These weak interactions (the bond parameters of hydrogen bonds listed in Table 2) improved the stabilization of the unit cell of **2** (Figure S2).

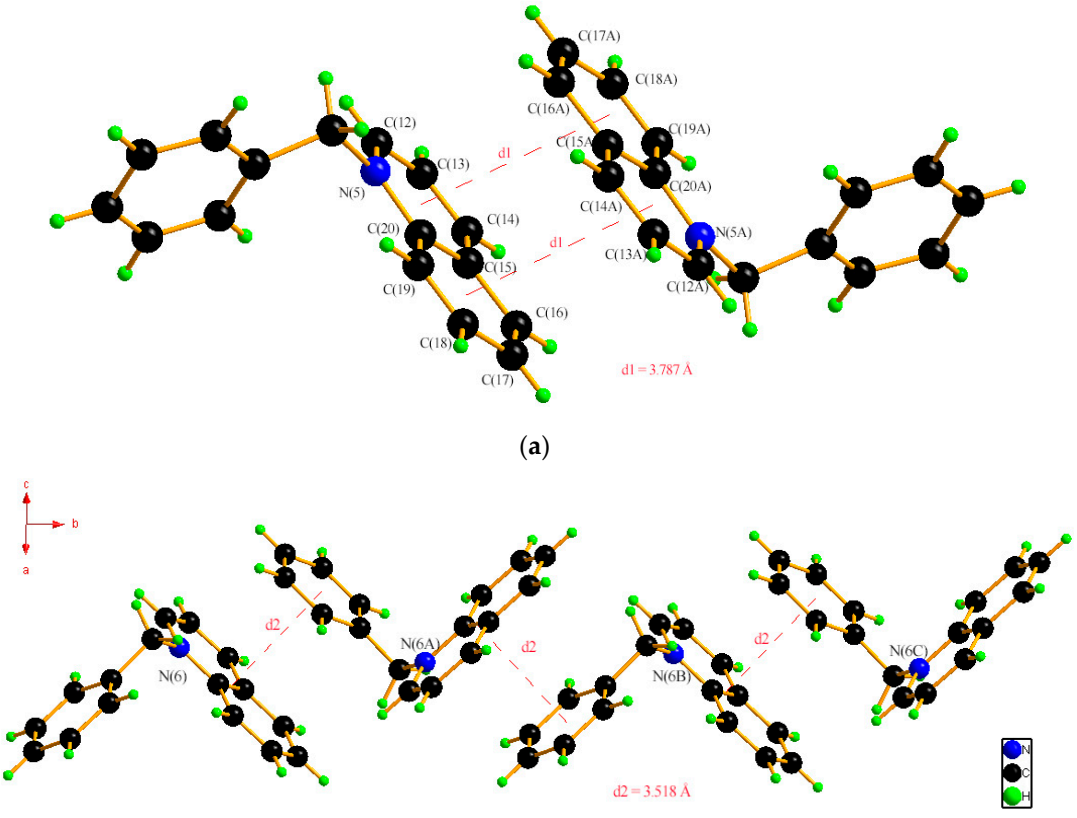

Figure 3. (**a**) The cations (C_1) form a dimer through π···π weak interactions between the quinoline rings of **2**. (**b**) The cations (C_2) form a chain structure via π···π weak interactions between the quinoline and benzyl rings of **2**.

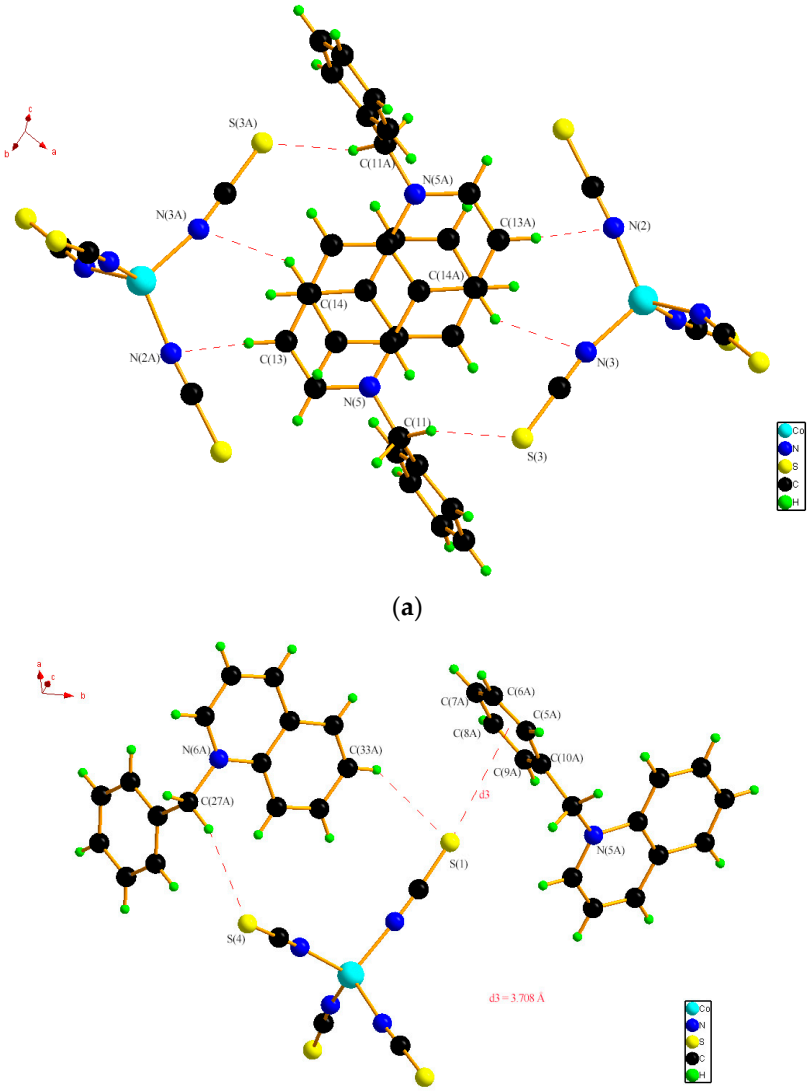

Figure 4. (**a**) The cationic dimers with two $[Co(NCS)_4]^{2-}$ anions formed an alliance through C–H···N and C–H···S hydrogen bonds of **2**. (**b**) The S···π and C–H···S interactions between the anions and cations of **2**.

By comparing the packing structures of (**1**), (**2**) and $[4NO_2BzPy]_2[Co(SCN)_4]$ [24], it was found that when the anion was identical, the aromatic rings of the cation changed from pyridine to a quinoline ring, or a *para*-substituted group in the benzyl ring changed from H to NO_2 groups, the anion stacking mode, the dihedral angles (θ_1, θ_2, and θ_3), the cations stacking mode and the weak interactions of the cations and anions were significantly different.

The grown crystals of **1** and **2** were finely powered and subjected to powder XRD analysis by employing a Bruker D8 advance power X-ray diffractometer. The powdered samples were scanned over a range of 2θ values 10°–50° in steps of 0.02° at room temperature. As seen in Figure 5, the sharp nature of the peaks in the XRD patterns and the consistency of most of the peak positions in powder XRD and simulated XRD patterns from single crystal XRD using Mercury software from the Cambridge Structural Database System indicates the purity and excellent crystallinity of the grown crystals of **1** and **2**.

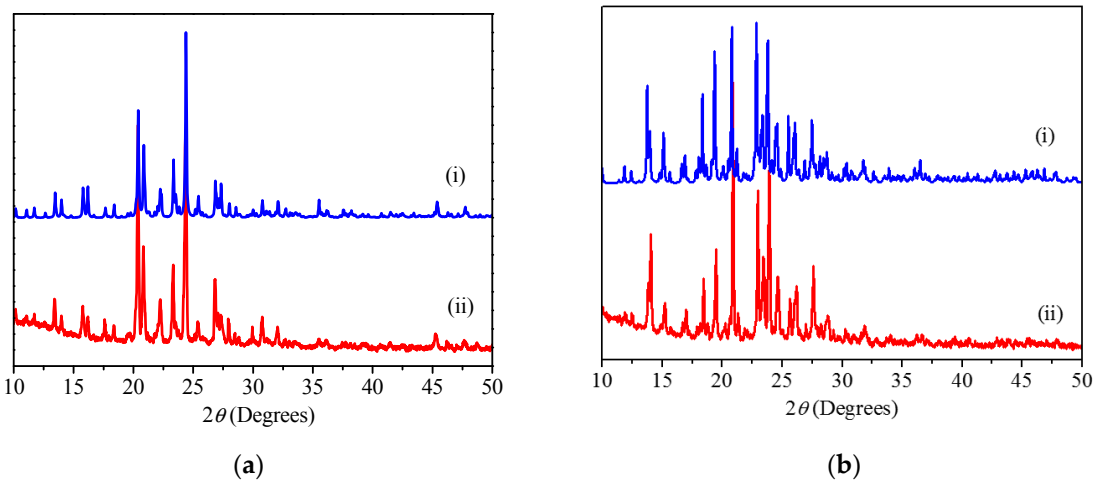

Figure 5. Simulated and experimental powder XRD patterns of **1** (**a**) and **2** (**b**): (i) calculated from single crystal structural analysis (blue line) and (ii) experimental (red line).

2.2. UV-Vis Spectra

The UV-Vis absorption spectra (Figure 6) of **1** and **2** in MeCN (1.0×10^{-6} mol L^{-1}) in the region of 220–800 nm are attributed to the anionic portions of these solids. The characteristic bands at 626, 319, 254 nm for **1** (Figure 6a) and 625, 318, 237 nm for **2** (Figure 6b), are assigned as d→d, L→L* and L(π)→M, respectively, and are basically similar to those observations in $[4NO2BzPy]_2[Co(NCS)_4]$ [24].

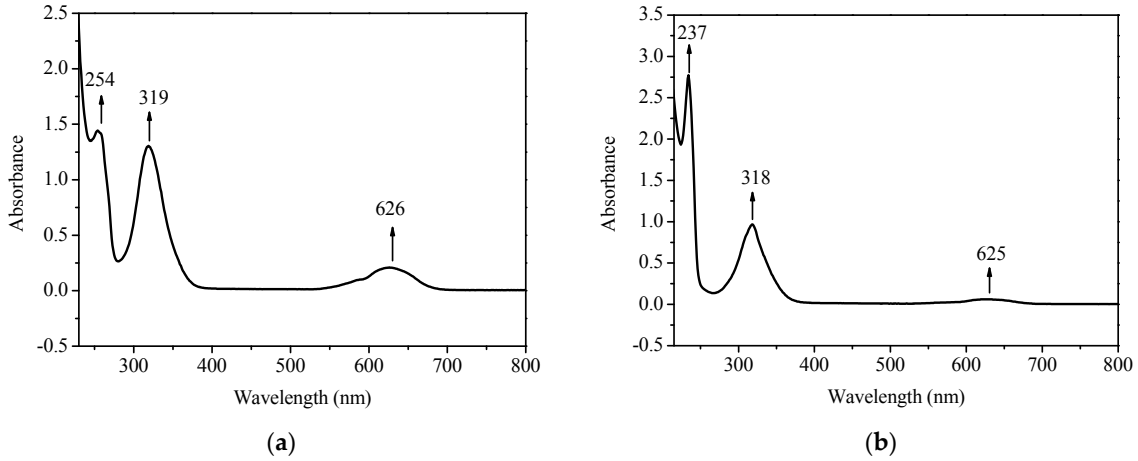

Figure 6. UV-Vis spectra of **1** (**a**) and **2** (**b**) in MeCN.

2.3. Luminescent Properties

The luminescent properties of the two solids and the intermediate were all investigated in a solid state at room temperature (the intermediates [BzPy]Br (Benzyl pyridinium bromide) of **1** do not obtain solid fluorescence as it is semi-solid state at room temperature). As seen in Figure 7a, upon excitation at 241 nm, compound **1** showed two main luminescent emission peaks at 395 nm and 290 nm, while the main emission bands of both **2** and intermediate [BzQl]Br were found at 289 nm and 394 nm (Figure 7b), which may be attributed to the π*→π or n→π transition [27]. In addition, compounds **1** and **2** exhibited a strong emission band at 408 nm and a relatively weak emission band at 448 nm, which may be tentatively assigned to the metal-to-ligand charge transfer band between the Co(II) and the unoccupied π* orbitals of the isothiocyanate groups [28]. It is noteworthy that the luminescence intensity of λ_{max} in **2** (186.9 a.u) is much stronger than the intermediate [BzQl]Br (benzyl quinolinium

bromide) (28.23 a.u), which may be primarily attributed to the C–H···S, and C–H···N hydrogen bond interactions between the $[Co(NCS)_4]^{2-}$ anions and $[BzQl]^+$ cations [29].

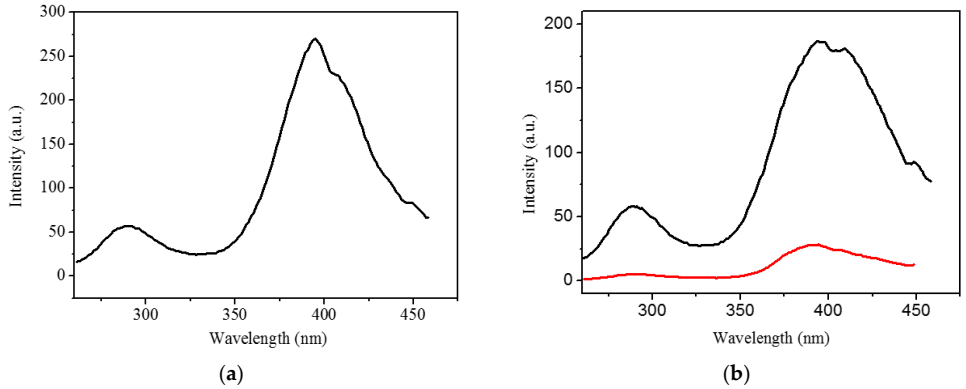

Figure 7. (**a**) Emission spectrum of **1** in a solid state at room temperature. (**b**) Emission spectra of **2** (black) and [BzQl]Br (red) in a solid state at room temperature.

2.4. Magnetic Properties

The crushed crystals of **1** and **2** were used to collect the variable-temperature (2–300 K) magnetic susceptibility data under a field of 2000 Oe. Plots of χ_m and $\chi_m - 1$ versus T are shown in Figure 8a for **1** and Figure 8b for **2**, while the plots of $\chi_m T$ versus T are shown in Figure S3a for **1** and Figure S3b for **2**. The $\chi_M T$ value of **1** at 300 K was 2.457 emu K mol^{-1}, which was slightly larger than the spin-only value of high-spin Co(II) (S = 3/2) at 1.875 emu K mol^{-1}, indicating a contribution of the orbital momentum typical for the $^4T_{1g}$ ground state [30,31]. As the temperature was lowered, first, the $\chi_M T$ product smoothly decreased to 2.255 emu K mol^{-1} around 34 K, then sharply decreased to a low value (1.132 emu K mol^{-1}) at 2.0 K (Figure S3a**)**, indicative of an antiferromagnetic exchange. The data in ${\chi_M}^{-1}$ versus T plot is well fitted by the Curie–Weiss law (the solid line in Figure 8a) with the fitting parameters of C = 2.459 emu K mol^{-1} and $\theta = -3.641$ K. The magnetic behavior of **2** also exhibited a very weak antiferromagnetic exchange interaction, and the best fit (the red solid line in Figure 8b) for the data in ${\chi_M}^{-1}$ versus T plot in the temperature range 2–300 K using the Curie–Weiss law was C = 2.410 emu K mol^{-1}, and $\theta = -1.295$ K. The magnetic behaviors of **1** and **2** are in accordance with their crystal structures, and similar to that in [4NO2BzPy][Co(NCS)$_4$] [24]. Due to the large Co–Co distances between the neighboring centers, the magnetic behavior was due to single ion anisotropy with some contribution of antiferromagnetic exchange between the Co(II) centers. The magnetic coupling can be mediated through super-exchange interaction across the isothiocyanate orbitals, as well as the C–H···S, and C–H···N hydrogen bonds between the anion and the cation [31,32].

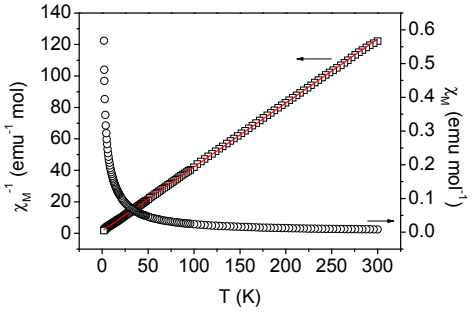

Figure 8. *Cont.*

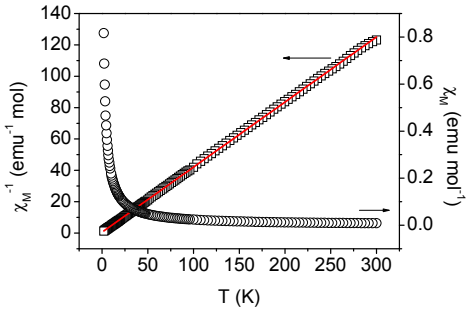

(**b**)

Figure 8. (**a**) Plots of χ_m and $\chi_m{}^{-1}$ versus *T* for **1**. (**b**) Plots of χ_m and $\chi_m{}^{-1}$ versus *T* for **2**. The solid lines are reproduced from the theoretical calculations and detailed fitting procedure described in the text.

3. Materials and Methods

3.1. Materials

Benzyl bromide, pyridine, quinoline, $CoCl_2{\cdot}6H_2O$, KSCN and other reagents were purchased from commercial sources and used without further purification. Benzyl pyridinium bromide ([BzPy]Br) and benzyl quinolinium bromide ([BzQl]Br) were prepared using the published methods in Reference [33].

3.2. Syntheses and Crystal Growth Method

Compound **1**: $[BzPy]_2[Co(NCS)_4]$ (the synthetic route is shown in Figure 9). A methanol solution (10 mL) of KSCN (0.20 g, 2 mmol) was added to a methanol solution (10 mL) of $CoCl_2{\cdot}6H_2O$ (0.12 g, 0.5 mmol), stirred and the mixture was stirred again for 45 min at room temperature. Next, then 20 mL methanol solution of [BzPy]Br (0.25 g, 1 mmol) was dropped into the mixture, cooled down for a further 1.5 h when all of the [BzPy]Br was added. The product was collected via filtration, wasted with cool methanol and diethyl ether, and air-dried. Yield: 82%. *Anal*. Calc. for $C_{28}H_{24}N_6CoS_4$: C, 53.24; H, 3.83; N, 13.30%; Found: C, 53.29; H, 3.95; N, 13.22%. IR spectrum (cm^{-1}): 3057m (ν_a-H), 2920m ($\nu_{as}CH_2$), 2855m (ν_sCH_2), 2069s (νC≡N), 1631m (νC=C), 1581s (νC=C), 1486m (νC=C), 1454m (νC=C), 1164s (ϱCH_2), 739m (δC–H), and 678m (δC–H). UV-Vis spectrum (nm): 254, 319, 626.

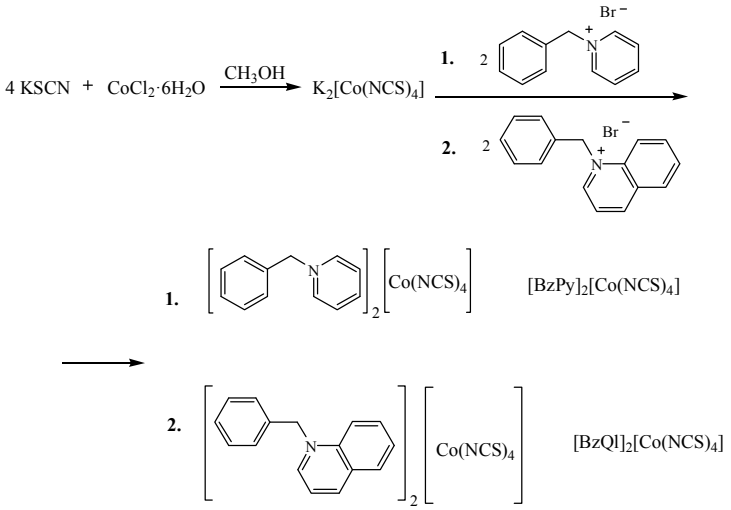

Figure 9. Synthetic route of the two complexes.

A similar procedure used to make Compound **1** was used to prepare Compound **2**. Yield: 79%. *Anal*. Calc. for $C_{36}H_{28}N_6CoS_4$: C, 59.09; H, 3.86; N, 11.48%; Found: C, 59.15; H, 4.01; N, 11.56%. IR spectrum (cm^{-1}): 3087m (ν_{as}C–H), 2923m ($\nu_{as}(CH_2)$), 2848m (ν_sCH_2), 2065s (νC≡N), 1626m (νC=C), 1589s (νC=C), 1521m (νC=C), 1452m (νC=C), 1157s, 768m (δC–H), 719m (δC–H). UV-Vis spectrum (nm): 237, 318, 625.

The blue crystals suitable for X-ray structural analysis were obtained by evaporating the MeOH solution of **1** and **2** for around two weeks at room temperature.

3.3. Characterization Technique

Elemental analyses (carbon, hydrogen, and nitrogen) were performed using a Perkin-Elmer (Massachusetts, MA, USA) Model 240C elemental analyzer. IR spectra were recorded on a Nicolet (Wisconsin, WI, USA) FT-IR spectrophotometer in 4000–400 cm^{-1} regions with a KBr pellet. UV-Vis spectra were recorded (in acetonitrile) on a Shimadzu (Tokyo, Japan) UV-2500 spectrophotometer in the region of 250–800 nm. The power XRD pattern was analyzed by a Bruker D8 Advance X-ray diffractometer (λ = 1.5406 Å). Single crystal XRD data were collected at room temperature using a Bruker SMART APEX instrument (Mo Kα radiation, λ = 0.71073 Å) for **1** and **2**. Cell parameters were retrieved using SMART software [34] and refined using SAINTPlus (Göttingen, Germany) software [35] on all observed reflections. Data reductions were also performed using the SAINTPlus software. The structure was solved by direct method and refined by the least-squares methods on F^2 using the SHELXTL (Göttingen, Germany) program package [36]. All non-hydrogen atoms were refined anisotropically. Hydrogen atoms were located in the Fourier map and their positions refined with fixed isotropic thermal parameters. Details of the data collection, refinement and crystallographic data are summarized in Table 3.

Table 3. Crystal data and structure refinement for **1** and **2**.

Compounds	1	2
Empirical formula	$C_{28}H_{24}N_6CoS_4$	$C_{36}H_{28}N_6CoS_4$
Formula weight	631.70	731.81
Crystal system	Monoclinic	Monoclinic
Space group	$P2_1/c$	$P2_1/n$
a/Å	8.749(1)	16.029(3)
b/Å	20.062(3)	12.731(2)
c/Å	17.527(2)	19.010(3)
β/°	96.28(1)	111.29(1)
Volume, Å^3	3058.0(7)	3614.7(10)
Z	4	4
Density (calculated), g/cm^3	1.372	1.345
Absorption coefficient, mm^{-1}	0.862	0.740
F(000)	1300	1508
Crystal size/mm^3	0.13 × 0.17 × 0.21	0.11 × 0.15 × 0.19
Reflections collected	26,736	25,478
Independent reflections	5676 (R_{int} = 0.069)	6353 (R_{int} = 0.037)
Data/restraints/parameters	5676/0/352	6353/0/424
Goodness of fit on F^2	1.000	1.067
Final R indices [$I > 2\sigma$ (I)]	$R1$ = 0.0480, $wR2$ = 0.0921	$R1$ = 0.0462, $wR2$ = 0.1199
Final R indices (all data)	$R1$ = 0.1034, $wR2$ = 0.1023	$R1$ = 0.0726, $wR2$ = 0.1370
Largest Diff Peak and hole (e Å^{-3})	0.232 and −0.357	0.630 and −0.510

3.4. Fluorescence Emission Spectra Measurements

Solid-state emission spectra upon excitation at 241 nm were recorded for the solid samples loaded into a sample cell (1 cm diameter) which was then fixed on a bracket at room temperature with a Hitachi F-7000 (Tokyo, Japan) fluorescence spectrophotometer. The excitation and emission slits

used for the measurement of the solid state of the crystals were 2.5 and 5.0 nm wide, the scan speed was 240 nm/min^{-1}, and the scan voltage was 400 V.

3.5. Magnetic Properties Measurements

Variable-temperature magnetic susceptibility measurements were carried out for **1** and **2** in the 2–300 K temperature range at a magnetic field of 0.2 T on ground polycrystalline samples with a Quantum Design MPMS-XL-7 (San Diego, CA, USA) super-conducting quantum interference device (SQUID) magnetometer. Samples were prepared by finely grinding single crystals into a powder and packing the powder into a gelatin capsule with weights of 34.36 mg and 60.40 mg for **1** and **2**, respectively. The susceptibility data were corrected for the diamagnetic contributions deduced by the use of Pascal's constant tables.

4. Conclusions

In summary, two new hybrid organic-inorganic molecular solids: (**1**) $[BzPy]_2[Co(NCS)_4]$ and (**2**) $[BzQl]_2[Co(NCS)_4]$ ($[BzPy]^+$ = Benzyl pyridinium, $[BzQl]^+$ = Benzyl quinolinium) were obtained and characterized. The crystal structural analysis revealed that two molecular metals crystallized in the monoclinic space group $P2_1/c$ of **1** and $P2_1/n$ of **2**. The cations formed a dimer through weak C–H$\cdots\pi/\pi\cdots\pi$ interactions in **1** and **2**, and the adjacent cation (containing the N(6) atom) in **2** formed a columnar structure through $\pi\cdots\pi$ weak interactions between the quinoline and benzene rings. The anions of **1** formed a layer structure via short S$\cdots$Co interactions. The anion (A) and cation (C_1) were arranged alternatively into a column in the sequence of $\cdots A-C_1C_1-A-C_1C_1-A\cdots$ for **1**, while in **2**, the two anions with a cationic dimer formed an alliance through the C–H$\cdots\pi$, C–H$\cdots$S and C–H$\cdots$N hydrogen bonds. The S$\cdots\pi$ weak interaction was found in **1** and **2**. So weak $p\cdots\pi/\pi\cdots\pi$ stacking interactions and hydrogen bonds play an important role in the arrangement of the structural units of molecular solids. Two molecular solids showed a broad fluorescence emission around 400 nm and weak antiferromagnetic coupling behavior.

Supplementary Materials: The following are available online at www.mdpi.com/2073-4352/7/3/92/s1, Figure S1: The packing diagram of **1** as viewed along *a*-axis, Figure S2: The packing diagram of **2** as viewed along *a*-axis, Figure S3: Plots of $\chi_m T$ *versus* *T* for **1** (**a**) and **2** (**b**).

Acknowledgments: This research was supported by the National Natural Science Foundation of China (No. 51301204), the National Key Research and Development Program of China (No. 2016YFB0700304), and the Science and Technology Project of Guangdong Science and Technology Department (No. 2014A010105037).

Author Contributions: Zheng Zhang conceived and designed the experiments, undertook structural analyses and wrote the manuscript. Junwei Xu determined the crystal structures. Sisi Yan conducted XRD study. Yangli Chen conducted spectral study. Zhuo Chen and Yan Wang contributed conceptual details and supported this study. Chunlin Ni was the advisor on this research and checked the analysis of the results and revised the manuscript.

Conflicts of Interest: The authors declare no conflict of interest.

References

1. Wang, K.; Stiefel, E.I. Toward separation and purification of olefins using dithiolene complexes: An electrochemical approach. *Science* **2001**, *291*, 106–109. [CrossRef] [PubMed]
2. Tomoyuki, A.; Takayoshi, N. Control of assembly and magnetism of metal-dmit complexes by supramolecular cations. *Coord. Chem. Rev.* **2001**, *226*, 3–9.
3. Robertson, N.; Cronin, L. Metal *bis*-1,2-dithiolene complexes in conducting or magnetic crystalline assemblies. *Coord. Chem. Rev.* **2002**, *227*, 93–127. [CrossRef]
4. Desiraju, G.R. Crystal engineering: From molecule to crystal. *J. Am. Chem. Soc.* **2013**, *135*, 9952–9967. [CrossRef] [PubMed]
5. Shapiro, A.; Landee, C.P.; Turnbull, M.M.; Jornet, J.; Deumal, M.; Novoa, J.J.; Robb, M.A.; Lewis, W. Synthesis, structure, and magnetic properties of an antiferromagnetic spin-ladder complex: Bis(2,3-dimethylpyridinium) tetrabromocuprate. *J. Am. Chem. Soc.* **2007**, *129*, 952–959. [CrossRef]

6. Li, L.X.; Turnbull, M.M. Synthesis, structure, and magnetic behavior of bis(2-amino-5-fluoropyridinium) tetrachlorocuprate(II). *Inorg. Chem.* **2007**, *46*, 11254–11265. [CrossRef] [PubMed]
7. Vela, S.; Deumal, M.; Ribas-Arino, J.; Novoa, J.J. Tracing the sources of the different magnetic behavior in the two phases of the bistable $(BDTA)_2[Co(mnt)_2]$ compound. *Inorg. Chem.* **2012**, *51*, 8646–8648. [CrossRef] [PubMed]
8. Savard, D.; Leznoff, D.B. Synthesis, structure and light scattering properties of tetraalkylammonium metal isothiocyanate salts. *Dalton Trans.* **2013**, *42*, 14982–14991. [CrossRef] [PubMed]
9. Walker, I.M.; McCarthy, P.J. Charge-transfer spectra and photochemistry of the hexakis(isothiocyanato) ferrate(III) ion at cryogenic temperatures in diluent crystals. *Inorg. Chem.* **1984**, *23*, 1842–1845. [CrossRef]
10. Kaye, S.S.; Long, J.R. Hydrogen storage in the dehydrated prussian blue analogues $M3[Co(CN)6]_2$ (M = Mn, Fe, Co, Ni, Cu, Zn). *J. Am. Chem. Soc.* **2005**, *127*, 6506–6507. [CrossRef] [PubMed]
11. Mrozinski, J.; Klak, J.; Kruszynski, R. Crystal structure and magnetic properties of the 1D bimetallic thiocyanate bridged compound: {(CuL1)[Co(NCS)(4)]}(L-1 = N-rac-5,12-Me-2-[14]-4,11-dieneN(4)). *Polyhedron* **2008**, *27*, 1401–1407. [CrossRef]
12. Chattopadhyay, S.; Bhar, K.; Das, S.; Chantrapromma, S.; Fun, H.K.; Ghosh, B.K. Syntheses, structures and properties of homo- and heterobimetallic complexes of the type [Zn(tren)NCS](2)[M(NCS)(4)] [tren = tris(2-aminoethyl)amine; M = Zn, Cu]. *J. Mol. Struct.* **2010**, *967*, 112–118. [CrossRef]
13. Quan, Y.P.; Yin, P.; Han, N.N.; Yang, A.H.; Gao, H.L.; Cui, J.Z.; Shib, W.; Cheng, P. Novel hetero-polynuclear metal complexes (CuL)(3)[Mn(NCS)(5)](2) and (NiL)(3)[Mn(NCS)(5)](2) containing trigonal bipyramidal geometric [Mn(NCS)(5)](3-) as bridging ligand. *Inorg. Chem. Commun.* **2009**, *12*, 469–472. [CrossRef]
14. Li, L.L.; Yuan, R.X.; Liu, L.L.; Ren, Z.G.; Zheng, A.X.; Cheng, H.J.; Li, H.X.; Lang, J.P. Formation of [CuSCN](n)-Based topological structures via a family of flexible benzimidazolyl-based linkers with different spacer lengths. *Cryst. Growth Des.* **2010**, *10*, 1929–1938. [CrossRef]
15. Zhang, H.; Wang, X.M.; Zhang, K.C.; Teo, B.K. Molecular and crystal engineering of a new class of inorganic cadmium-thiocyanate polymers with host–guest complexes as organic spacers, controllers, and templates. *Coord. Chem. Rev.* **1999**, *183*, 157–195. [CrossRef]
16. Ghazzali, M.; Langer, V.; Oehrstroem, L. The role of intermolecular interactions in the assemblies of FeII and CoII tetrakis-isothiocyanatometalates with tris(1,10-phenanthroline)-RuII: Crystal structures of two dual-metal assemblies featuring octahedral cationic and tetrahedral anionic modules. *J. Solid State Chem.* **2008**, *181*, 2191–2198. [CrossRef]
17. Ohba, M.; Okawa, H. Synthesis and magnetism of multi-dimensional cyanide-bridged bimetallic assemblies. *Coord. Chem. Rev.* **2000**, *198*, 313–328. [CrossRef]
18. Chen, H.J.; Zhang, L.Z.; Cai, Z.G.; Yang, G.; Chen, X.M. Organic-inorganic hybrid materials assembled through weak intermolecular interactions: Synthesis, structures and non-linear optical properties of [4,4′-bipyH(2)][M(NCS)(4)] (M = Mn2+, Co2+ or Zn2+; 4,4′-bipy=4,4′-bipyridine). *J. Chem. Soc. Dalton Trans.* **2000**, *14*, 2463–2466. [CrossRef]
19. Chen, X.; Chen, W.Q.; Han, S.; Liu, J.F.; Zhou, J.R.; Yu, L.L.; Yang, L.M.; Ni, C.L.; Hu, X.L. Two hybrid materials self-assembly from tetra(isothiocyanate)cobalt(II) dianion and substituted benzyl triphenylphosphinium. *J. Mol. Struct.* **2010**, *984*, 164–169. [CrossRef]
20. Chen, X.; Dai, S.L.; Cheng, Z.P.; Liang, L.B.; Han, S.; Liu, J.F.; Zhou, J.R.; Yang, L.M.; Ni, C.L. Syntheses, crystal structures, and magnetic properties of two hybrid materials self-assembly from tetra(isothiocyanate)cobalt(II) anion and substituted benzyl triphenylphosphinium. *Synth. React. Inorg. Met. Org. Nano Met. Chem.* **2012**, *42*, 987–993. [CrossRef]
21. Chen, W.Q.; Su, L.J.; Cai, X.Q.; Yang, J.J.; Qian, Y.L.; Liu, X.P.; Yang, L.M.; Zhou, J.R.; Ni, C.L. Syntheses, crystal Structures, and magnetic properties of two meta-substituted benzyl triphenylphosphinium tetra(isothiocyanate)cobaltate(II) complexes. *Synth. React. Inorg. Met. Org. Nano Met. Chem.* **2014**, *44*, 980–985. [CrossRef]
22. Ye, H.Q.; Su, L.J.; Chen, X.X.; Liao, X.; Liu, Q.T.; Wu, X.Y.; Zhou, J.R.; Yang, L.M.; Ni, C.L. Syntheses, crystal structures, weak interaction, magnetic and luminescent properties of two new organic-inorganic molecular solids with substituted chlorobenzyl triphenylphosphinium and tetra (isothiocyanate)cobalt(II) anion. *Synth. Met.* **2015**, *199*, 232–240. [CrossRef]

23. Ye, H.Q.; Xie, J.L.; Yu, J.Y.; Liu, Q.T.; Dai, S.L.; Huang, W.Q.; Zhou, J.R.; Yang, L.M.; Ni, C.L. Syntheses, crystal structures, luminescent properties of two new molecular solids with tetra(isothiocyanate)zinc(II) and substituted benzyl triphenylphosphonium cations. *Synth. Met.* **2014**, *197*, 99–104. [CrossRef]
24. Ye, H.Q.; Li, Y.Y.; Huang, R.K.; Liu, X.-P.; Chen, W.Q.; Zhou, J.R.; Yang, L.M.; Ni, C.L. Unusual layer structure in an ion-paired compound containing tetra(isothiocyanate) cobalt(II) dianion and 4-Nitrobenzylpyridinium: Crystal structure and magnetic properties. *J. Struct. Chem.* **2014**, *55*, 691–696. [CrossRef]
25. Allinger, N.L.; Zhou, X.F.; Bergsma, J. Molecular mechanics parameters. *J. Mol. Struct. Theochem.* **1994**, *31*, 269–283. [CrossRef]
26. Batsanov, S.S. Van der Waals Radii of Elements. *Inorg. Mater.* **2001**, *37*, 871–885. [CrossRef]
27. Ma, L.F.; Wang, L.Y.; Hu, J.L.; Wang, Y.Y.; Yang, G.P. Syntheses, structures, and photoluminescence of a series of d(10) coordination polymers with R-Isophthalate (R = –OH, $–CH_3$, and $–C(CH_3)(3)$). *Cryst. Growth Des.* **2009**, *9*, 5334–5342. [CrossRef]
28. Jiao, C.H.; He, C.H.; Geng, J.C.; Cui, G.H. Syntheses, structures, and photoluminescence of three cadmium(II) coordination polymers with flexible bis(benzimidazole) ligands. *J. Coord. Chem.* **2012**, *65*, 2852–2861. [CrossRef]
29. Ashenhurst, J.; Wu, G.; Wang, S.N. Syntheses, Structures, Solution, and Solid-State ^{27}Al NMR Studies of Blue Luminescent Mononuclear Aluminum Complexes: Al(7-azain)$_2$(7-azain-H)(CH_3), Al(7-azain)$_3$(7-azain-H), and Al(7-azain)(7-azain-H)($OCH(CF_3)_2$)$_2$ (7-azain-H) 7-azaindole). *J. Am. Chem. Soc.* **2000**, *122*, 2541–2547. [CrossRef]
30. Li, B.L.; Wang, X.Y.; Zhu, X.; Gao, S.; Zhang, Y. Synthesis, crystal structure and magnetic behavior of two cobalt coordination polymers with 1,2-bis(1,2,4-triazol-1-yl)ethane and dicyanamide. *Polyhedron* **2007**, *26*, 5219–5224. [CrossRef]
31. Wei, Y.Q.; Wu, K.C.; Broer, R.; Zhuang, B.T.; Yu, Y.F. A polymeric cobalt compound [Co(DCNT)(H_2O)](n) with novel topology: Synthesis, structure, luminescence, and magnetic property. *Inorg. Chem. Commun.* **2007**, *10*, 910–913. [CrossRef]
32. Holman, K.T.; Hammud, H.H.; Isber, S.; Tabbal, M. One-dimensional coordination polymer $[Co(H_2O)_4(pyz)](NO_3)_2 \cdot 2H_2O$ (pyz = pyrazine) with intra- and inter-chain H-bonds: Structure, electronic spectral studies and magnetic properties. *Polyhedron* **2005**, *24*, 221–228. [CrossRef]
33. Bulgarevich, S.B.; Bren, D.V.; Movshovic, D.Y.; Finocchiaro, P.; Failla, S. Conformational investigation of *N*-aralkylpyridinium ions by cotton-mouten effect method. *J. Mol. Struct.* **1994**, *317*, 147–155. [CrossRef]
34. SMART. *Brucker Molecular Analysis Research Tool*; Version 6.1; Bruker AXS: Madison, WI, USA, 2000.
35. SAINTPlus. *Data Reduction and Correction Program*; Version 6.01; Bruker AXS: Madison, WI, USA, 2000.
36. SHELXTL. *Structure Determination Software Programs*; Version 6.10; Shelddrick, G.M., Ed.; Bruker AXS Inc.: Madison, WI, USA, 2000.